



Evaluating SWOT's interferometric capabilities for mapping intertidal topography



Edward Salameh ^{a,*}, Damien Desroches ^b, Julien Deloffre ^a, Roger Fjørtoft ^b, Ernesto Tonatiuh Mendoza ^a, Imen Turki ^a, Laurent Froideval ^c, Romain Levaillant ^a, Simon Déchamps ^a, Nicolas Picot ^b, Benoit Laignel ^a, Frédéric Frappart ^d

^a Univ Rouen Normandie, Univ Caen Normandie, CNRS, M2C, UMR 6143, F-76000 Rouen, France

^b CNES, 18 Avenue Edouard Belin, CEDEX 9, 31401 Toulouse, France

^c Univ Caen Normandie, Univ Rouen Normandie, CNRS, M2C, UMR 6143, F-14000 Caen, France

^d ISPA, UMR1391 INRAE Bordeaux Science Agro, F-33140, Villenave d'Ornon, France

ARTICLE INFO

Edited by Menghua Wang

Keywords:
SWOT
Interferometry
Intertidal
Topography
Coastal areas
DEM

ABSTRACT

The Surface Water and Ocean Topography (SWOT) mission, originally designed for observing ocean and inland water bodies, can be a valuable tool for mapping the topography of intertidal flats. This study provides the first demonstration of SWOT's ability to measure intertidal topography using simultaneous interferometric acquisitions. Observations acquired between April and July 2023, during the calibration/validation (CALVAL) phase of the mission, were used. SWOT-derived intertidal Digital Elevation Models (DEMs) were generated from level-2 High-Rate Pixel Cloud (L2_HR_PIXC) products and compared to airborne and UAV LiDAR-derived DEMs. Our results indicate a high reliability of the SWOT observations with a mean absolute error lower than 0.49 m, reaching 0.13 m in specific areas. This validation confirms SWOT's contribution for coastal studies beyond water level mapping, showcasing its broader applicability in the monitoring and management of coastal and estuarine environments.

1. Introduction

Intertidal flats, characterized by their constantly evolving landscapes at the interface between land and sea, represent complex environments that require comprehensive study to fully understand their dynamic nature. The hydrodynamic forces drive changes in the morphology, influencing its shape and structure. These alterations in morphology, in turn, reciprocally impact the hydrodynamics within the system. This interplay constitutes what we know as morphodynamics (Masselink and Gehrels, 2015). Therefore, collecting intertidal topography data regularly is a necessity that allows to understand and manage intertidal flats that provide essential societal and economic services (Murray et al., 2019).

Satellites are the only logically viable tool for mapping intertidal topography at global scale while ensuring regular updating (Benveniste et al., 2019; Laignel et al., 2023). Development of spaceborne-based methods for measuring intertidal topography started three decades ago (Salameh et al., 2019). The waterline method, proposed by Mason

et al. (1995), is considered as one of the most efficient methods for such coastal applications. It extracts waterlines from a series of radar, or optical images acquired at different tidal stages, assigns elevation to these waterlines using in situ or modelled sea level information, and interpolates the leveled waterlines to produce a gridded intertidal Digital Elevation Model (DEM).

Intertidal topography can also be measured using Interferometric Synthetic Aperture Radar (InSAR) observations (Lee and Ryu, 2017). The InSAR technique is used to derive topographic information from the phase differences in at least two Single-Look Complex (SLC) SAR images, which are taken from different angles, known as primary and secondary images. This method is an established technique for generating DEMs for inland areas (Gens and Van Genderen, 1996). Nonetheless, the capacity to generate accurate intertidal DEMs through this approach requires a short temporal baseline (Salameh et al., 2019). Single-pass interferometric systems (using two antennas on the same platform) are designed to allow InSAR acquisitions without any temporal baseline, which is the case for the recently launched Surface Water and Ocean Topography

* Corresponding author.

E-mail address: edward.salameh@cnrs.fr (E. Salameh).

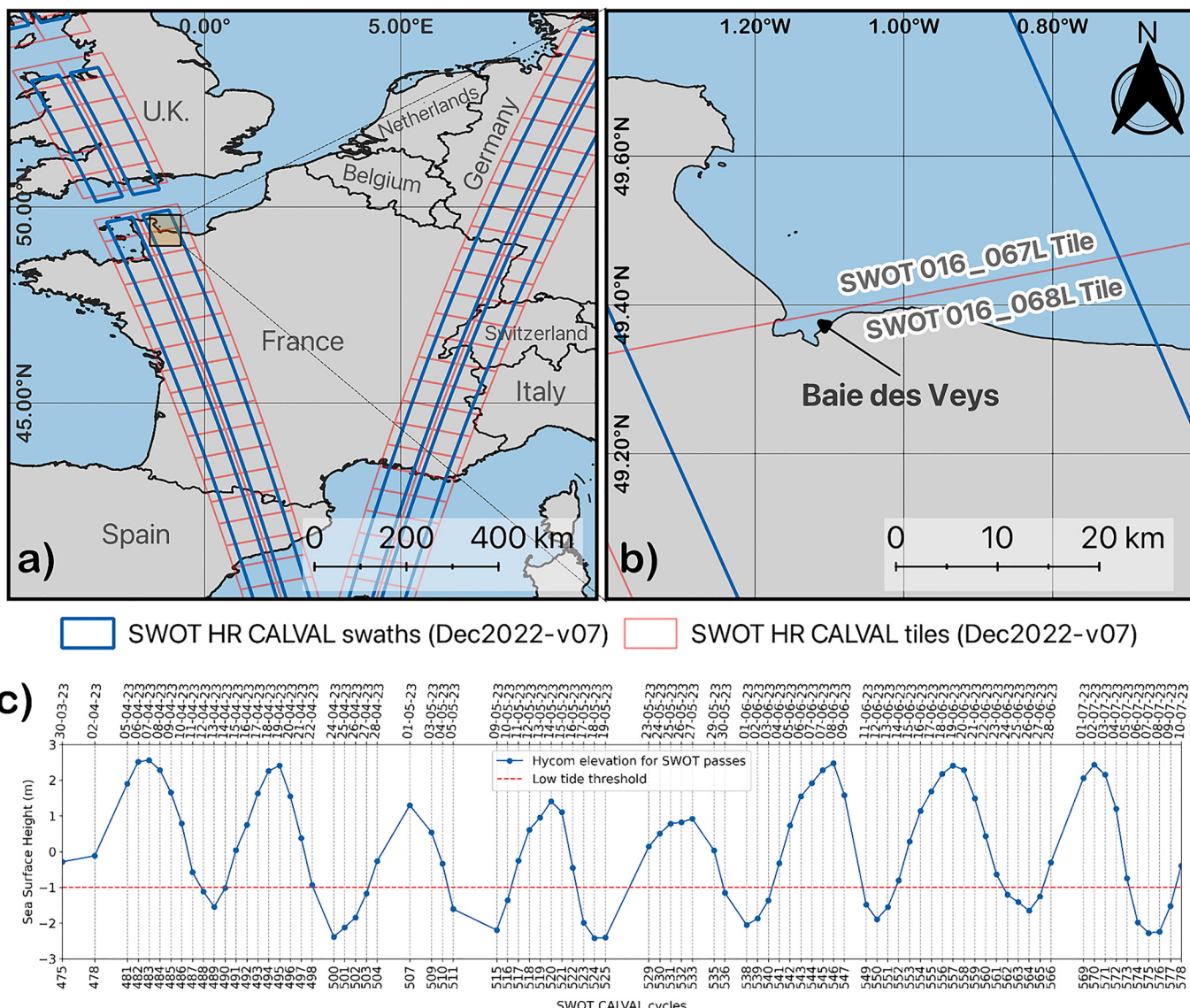


Fig. 1. (a) The Bay of Veys is located on the French coast of the English Channel, in Normandy. (b) It is encompassed in the SWOT HR CALVAL tiles 067 L and 068 L of pass 016. (c) The acquisition recorded between March 30th, 2023 (cycle 475) and July 9th, 2023 (cycle 577) covers the complete tidal cycle according to sea surface height provided by the Hycom model. 28 of the SWOT cycles were acquired at low tide.

(SWOT) mission (Fu et al., 2024).

The SWOT satellite, launched on December 16th, 2022, features an innovative wide-swath altimetry technology based on low-incidence single-pass InSAR acquisitions. With a mission to map the Earth water over the oceans and continental surfaces (Fu et al., 2024), SWOT offers new perspectives in monitoring the topography of intertidal flats, expanding its capabilities beyond its intended use. SWOT is expected to be able to exploit both the waterline and the direct InSAR methods to generate intertidal DEMs (Salameh et al., 2021). The InSAR method has the great advantage of only requiring a single acquisition at low tide to generate intertidal topography, compared to the waterline method which needs a series of images sampling adequately the whole tidal cycle, typically 3 to 4 months of data for SWOT's 21-day science orbit, according to Salameh et al. (2021).

This study aims to demonstrate SWOT's interferometric ability to measure the topography of intertidal areas and evaluate its performance. To achieve the above-mentioned goals, we used SWOT observations acquired during the calibration/validation (CALVAL) phase. SWOT-derived intertidal topography maps were compared to Unmanned Airborne Vehicle (UAV) and airborne LiDAR-derived

benchmark datasets. Furthermore, this study compares SWOT-derived topography to waterline-derived topography using Sentinel-1 and Sentinel-2 images.

2. The SWOT mission

SWOT is a joint project between NASA (National Aeronautics and Space Administration) and the French Space Agency CNES (Centre National d'Etudes Spatiales), with contribution from the Canadian Space Agency (CSA) and the United Kingdom Space Agency (UKSA), which carries the Ka-band Radar Interferometer (KaRIn) instrument. The latter is a bistatic SAR system operating at a frequency of 35.75 GHz (wavelength of 8.4 mm), with a pair of antennas separated by a 10-m boom observing the Earth's surface in a near-nadir look angles ranging between $\sim 1^\circ$ and $\sim 4^\circ$. One antenna emits radar signals, and both antennas receive the radar backscattered signals, offering a 120 km wide swath coverage, which includes 50 km from each side and a 20 km gap in the middle (Fjørtoft et al., 2014). KaRIn was designed to provide highly precise water level measurements over oceans, coastal, and continental surfaces. SWOT is also equipped with a conventional nadir

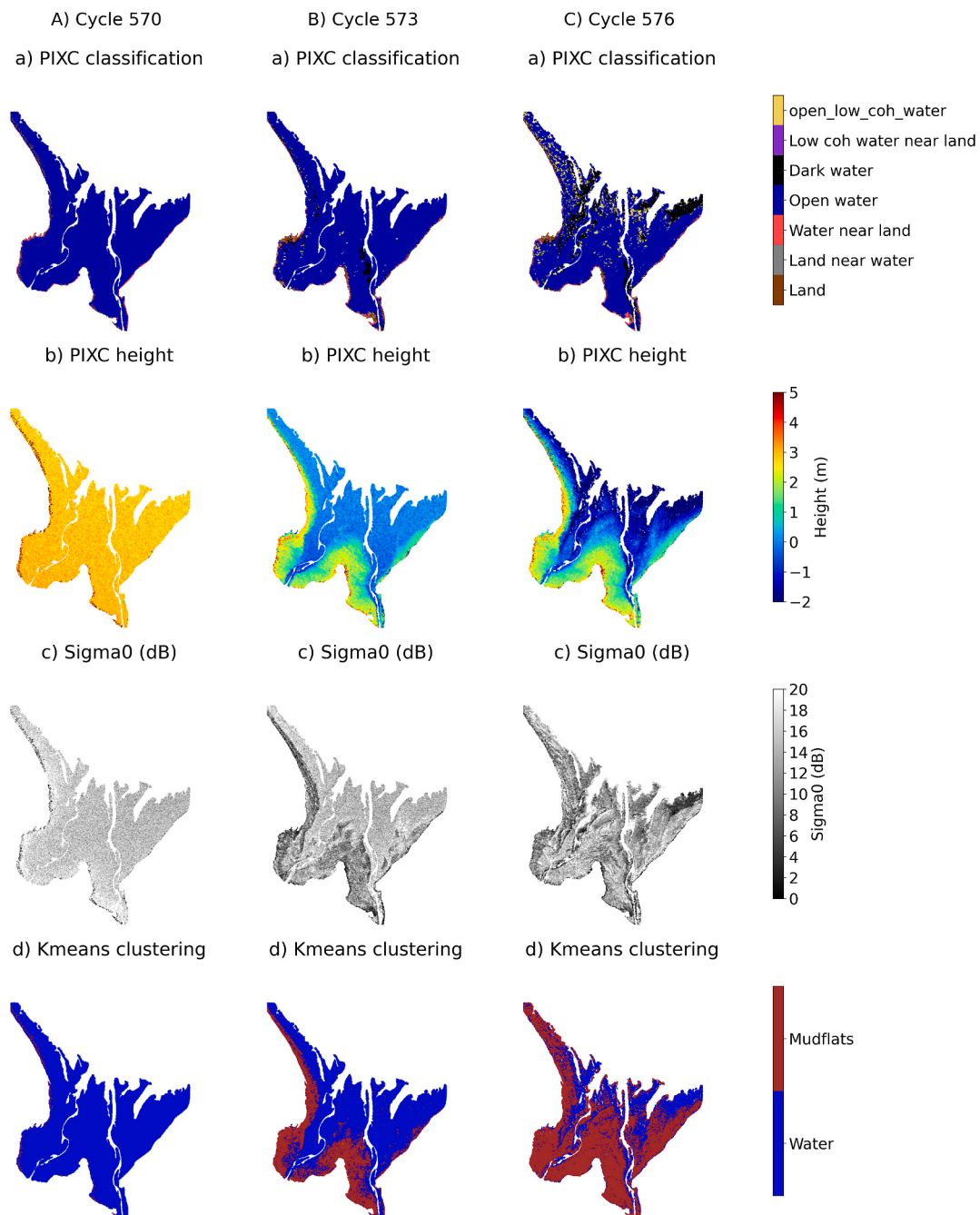


Fig. 2. Information provided in the SWOT pixel-cloud product – (a) classification, (b) height, and (c) σ_0 , as well as (d) k-means classification results based on heights and σ_0 which allow to separate mudflats from water.

altimeter suite providing measurements within the 20 km gap (Biancamaria et al., 2016). SWOT operates in a non-sun-synchronous orbit, with a 21-day (20.86455) repeat cycle at an altitude of 890.6 km and an inclination of 77.6° during the science phase (Aviso, 2023). During the first 6 months of the mission, SWOT was on a different orbital altitude (857.2 km) and a 1-day (0.99349) repeat cycle duration (Aviso, 2023). The first three months of this period were dedicated for engineering check-out, followed by three months for calibration and validation (Fu et al., 2024), known as the CALVAL phase, to ensure the performance of SWOT's systems and science instruments. During this CALVAL phase, SWOT operated in a 1-day repeat orbit with limited global coverage, providing data for a 3-month period, from March 30th to July 11th, 2023, (Aviso, 2023).

Since July 21st, 2023, SWOT has been producing data in its science

orbit (Aviso, 2023). Both CALVAL and science orbits share an inclination of 77.6° (Aviso, 2023). However, the number of orbits per cycle varies significantly, with 14 orbits per cycle for CALVAL and 292 orbits per cycle for the Science orbit (Aviso, 2023). SWOT has a High Rate (HR) and a Low Rate (LR) mode, with HR mode dedicated to continental water surfaces including coastal areas, whereas LR mode has global coverage but is mainly dedicated to ocean water surfaces. HR products are provided for areas included in SWOT's reloadable HR mask.

3. Study site

The Bay of Veys, a shallow estuarine embayment on the southern shore of the English Channel and part of the Bay of Seine, is a key site for the SWOT science team's coastal CALVAL activities. This bay, located

within the 1-day orbit swath, receives freshwater from the Aure, Douve, Taute, and Vire rivers, with the latter contributing with 40 % of the inflow (Grangeré et al., 2009; Lafforgue et al., 2018). The four rivers enter the bay via sluice gates, which operate with the tides, opening during the ebb tide and closing at flood tide (Lafforgue et al., 2018). Its environmental setup, characterized by a semi-diurnal macrotidal regime with tidal ranges reaching up to 8 m during spring tides, reveals an extensive, 37 km² intertidal area at low tide (Grangeré et al., 2009; Timsit et al., 2004). This area, extending 5 km offshore, features lower parts covered in sandy and muddy sediments and upper parts colonized by halophytic species like *Spartina anglica* (Deroïn, 2012; Timsit et al., 2004). The bay's configuration, including its polders and dikes, and the division of the intertidal zone into central, eastern, and western parts, make it an ideal location for evaluating SWOT's capabilities in mapping intertidal topography. The bay is completely covered by the left swath of SWOT's descending CALVAL pass number 16 (Fig. 1).

4. Datasets and methods

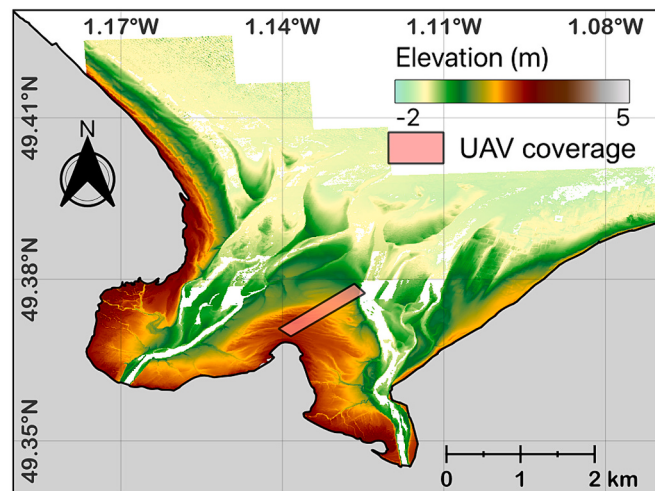
In this section, details on the datasets, their processing, and the methodologies employed for generating the DEMs from all types of sensors are described. All resulting DEMs are either directly referenced to or converted into the IGN69 vertical reference system.

4.1. SWOT observations and processing

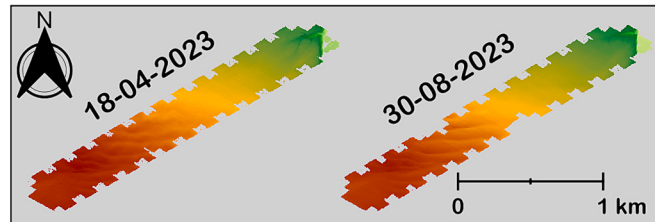
For assessing SWOT's interferometric abilities to measure the intertidal topography, the level 2 KaRIn HR pixel cloud product (L2_HR_PIXC) has been used. This product is generated within the SWOT HR reloadable mask that covers inland and coastal areas (JPL D-56411, 2023) following algorithms detailed in (JPL D-105504, 2023). The L2_HR_PIXC product is organized into tiles. Fig. 1 shows that the bay spans across two tiles in the CALVAL phase, 016_067L and 016_068L. The term pixel cloud is used, rather than point cloud, because different samples in the product have different surface area (projected pixel area on the ground) depending on the location of the sample (from nadir to the far-range swath edge). This product provides, for each sample (pixel), the geolocated height, class type (land, land near water, water near land, open water, dark water, low coherence water near land, open low coherence water), surface water area, and other parameters (JPL D-56411, 2023); Check the L2_HR_PIXC product Algorithm Theoretical Basis Documents (ATBD) (JPL D-105504, 2023) and Lobry et al. (2019) for more details about water detection. Only pixels detected as water, land pixels near detected water, and pixels considered to potentially represent water based on prior data, are kept in the L2_HR_PIXC products.

At low tides, the emerged intertidal bed, is generally classified as water due to the strong backscatter of these surfaces (compared to dry land), because of their high humidity and roughness at the scale of the Ka-band wavelength. This also allows to achieve an adequate interferometric coherence and therefore precise geolocated heights. The first step was to isolate the emerged intertidal mudflat pixels from land and water pixels. While the classification in the L2_HR_PIXC product does not contain any dedicated class for mudflats, backscattering coefficients (σ_0) from SWOT (Fig. 2.d), with the help of SWOT heights (Fig. 2.c), enabled the separation between water and mudflats. No manual selection of SWOT data was performed, however only pixels classified by SWOT as "open water" (class 4) were kept. As the SWOT tile covers extensive inland areas, a priori intertidal mask was used to remove open water pixels detected by SWOT over inland reservoirs (rivers, lakes, etc.). The priori intertidal mask was created using a Sentinel-1 image acquired on July 20th, 2023, at the lowest tide during the CALVAL phase. The isolation of mudflat pixels from the remaining open water pixels inside the intertidal mask was performed using a simple k-means unsupervised clustering based on heights and σ_0 from SWOT as inputs. k-means is a clustering algorithm that partitions a dataset into k distinct

a) IGN LiDAR HD intertidal DEM



b) UAV LiDAR intertidal DEMs



c) Waterline intertidal DEM

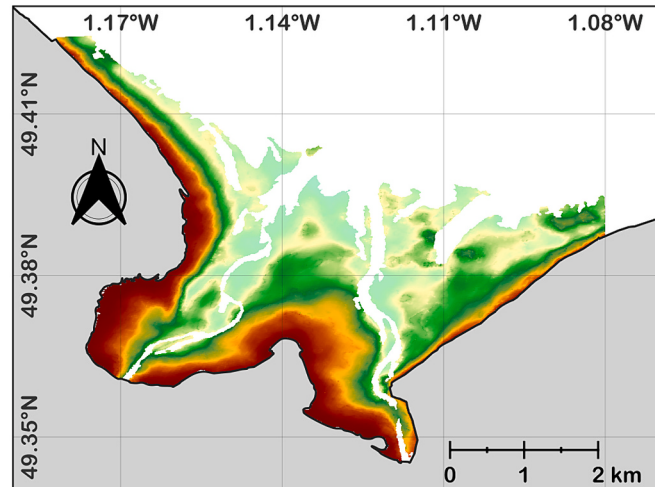


Fig. 3. Intertidal DEM of the Bay of Veys from (a) IGN LiDAR HD, (b) UAV LiDAR, and (c) the waterline method using Sentinel-1 and Sentinel-2 images.

clusters ($k = 2$ in this case; water and mudflats) by minimizing the mean square distance between points within each cluster and assigning each data point to the nearest cluster centroid (Arthur and Vassilvitskii, 2007). Fig. 2 shows examples of the L2_HR_PIXC product classification, height, and σ_0 parameters during high, mid, and low tides. It also shows the resulting k-means classification that allows to automatically extract mudflat pixels to use for intertidal DEM generation.

Pixels classified as mudflats are then extracted from all SWOT cycles (for all tidal stages) and used to generate several intertidal DEMs:

- A DEM generated from an aggregation of mudflat pixels extracted from all cycles.
- A DEM generated from an aggregation of mudflat pixels extracted from low tide cycles (using -1 m as threshold for low tide cycles; see Fig. 1).
- Single-pass DEMs for low tide cycles generated using mudflat pixels of the corresponding cycle without any aggregation of pixels from multiple passes.

All DEMs were generated on a regular 10-m grid by interpolating heights using the Inverse Distance Weighting (IDW) method (Shepard, 1968).

4.2. Benchmark datasets

4.2.1. LiDAR HD product

LiDAR HD is a French national program that aims to map the entire French territory in 3D using airborne LiDAR acquisitions. In the framework of LiDAR HD, the French national institute of geographic and forest information, formerly known as Institut Géographique National (IGN), produces and distributes LiDAR data as either raw or classified point clouds (IGN, 2022). The acquisitions are performed on $50\text{ km} \times 50\text{ km}$ blocks and provided as LAZ tiles of $1\text{ km} \times 1\text{ km}$ (IGN, 2023a). A geometric quality control is performed on the acquired data using control points (IGN, 2023a). The product guarantees a minimum planimetric precision of 50 cm (relative precision of 25 cm) and a minimum altimetric precision of 10 cm (relative precision of 5 cm) with a density of at least 10 points/m^2 (IGN, 2023a). The LiDAR HD project has indicated that coastal acquisitions are planned to coincide with low tides ensuring maximum coverage of intertidal areas (IGN, 2023). However, acquisition of seabed that requires a bathymetric LiDAR is not in the scope of the project (IGN, 2023). The Bay of Veys is located within the FD block (point cloud validated and available via diffusion-lidarhd.ign.fr) that has a 2223 km^2 area for which the acquisitions were made between August 29th and October 7th, 2022 (IGN, 2024), about 3 months ahead of SWOT's launch and 6 months before fully exploitable HR data are available. Over conterminous France the product is provided according to the RGF93/L-93 coordinate reference system (epsg:2154) and vertically referenced to the IGN69 datum (IGN, 2023a). The product provides a point cloud of x , y , z (and other parameters such as intensity and classification). A raster DEM was generated by averaging the LiDAR data points to $10 \times 10\text{ m}^2$ grid cells based on SWOT DEMs grid (Fig. 3.a). Grid cells with no data points were kept empty to ensure that the generated DEM that is compared to SWOT DEMs represents only areas where data were collected.

4.2.2. UAV LiDAR

Two UAV LiDAR surveys were conducted over a limited segment within the Bay (Fig. 3.a) using the DJI Zenmuse L1 LiDAR instrument mounted on a Matrice 300 RTK (Real Time Kinematic) quadcopter drone. Detailed information about the LiDAR instrument can be found on the manufacturer's website (www.dji.com/cz/zenmuse-l1/specs, 23 February 2023). High resolution data were acquired during low tide on April 18th and August 30th, 2023 (during the CALVAL phase). The drone flew at an altitude of 50 m at a speed of 1 m/s and a lateral overlap of 20 % , achieving a ground horizontal resolution of 1.36 cm and a density of 2828 points/m^2 . The data were processed using the DJI Terra 3D model reconstruction software that provided a high-resolution point cloud in WGS84 CRS and datum, which was resampled to 10 m resolution (using the same method used for LiDAR HD) and converted to IGN69 vertical reference system (Fig. 3.b).

4.2.3. Waterline-derived DEMs using Sentinel-1 and -2

The waterline method mentioned in the introduction and explained briefly was used to generate intertidal DEMs using the waterlines extracted from Sentinel-1 SAR imagery and Sentinel-2 multispectral

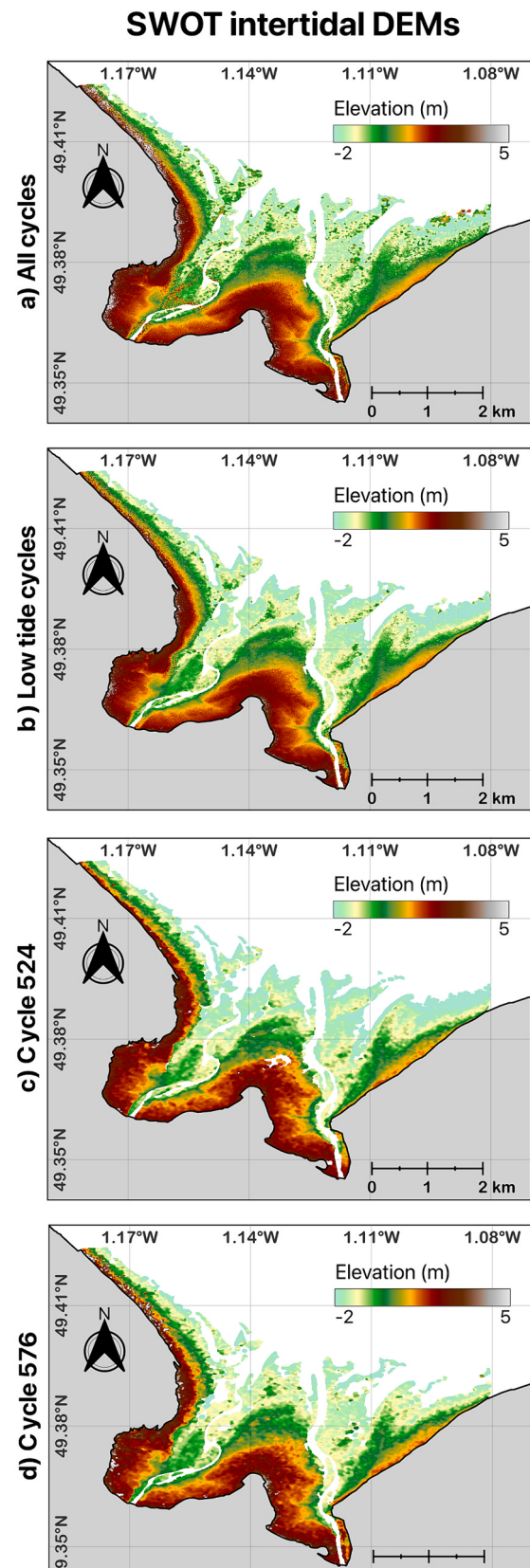


Fig. 4. SWOT intertidal DEMs obtained using observations from: (a) all cycles, (b) low tide cycles, (c) cycle 524, and (d) cycle 576.

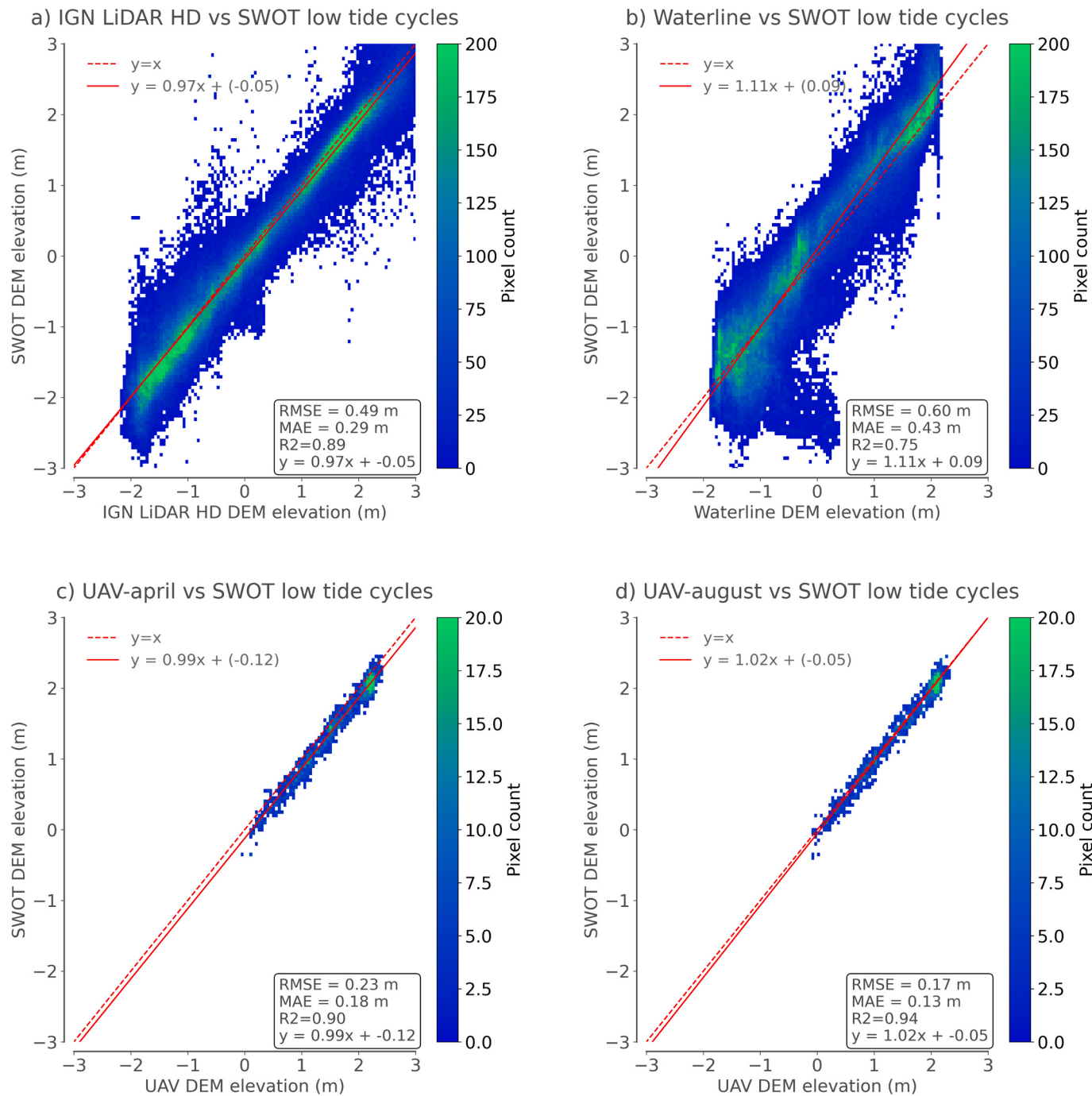


Fig. 5. Scatter plots between SWOT low tide cycles DEM and: (a) IGN LiDAR HD DEM, (b) waterline-derived DEM, (c) UAV-april DEM, and (d) UAV-august DEM.

imagery. The method used to build DEMs using the waterline method is the one developed by Salameh et al. (2020). The waterlines were extracted from images acquired during the CALVAL phase (March to July 2023). The extracted waterlines were leveled using the Hybrid Coordinate Ocean Model (HYCOM) circulation model (SHOM, 2014) and then interpolated to the same 10 m regular grid using the IDW method (Fig. 3.c).

5. Results and discussion

Several intertidal DEMs were generated from SWOT observations to fully assess its ability to accurately monitor intertidal topography. The first DEM derived from mudflat pixels extracted from all observed

CALVAL cycles (Fig. 4.a) (acquired almost daily during a 2-month period) offered an overview of the intertidal terrain, integrating morphological fluctuations across the whole acquisition period. This aggregated DEM exhibited consistent topographical features such as elevation gradients and key landforms (i.e. large channels, tidal creeks, ridges). The second DEM was generated exclusively from mudflat pixels captured during low tide cycles, offering a refined mapping of the intertidal topography at its most exposed state (Fig. 4.b). Lastly, a series of single-pass DEMs were generated, each mapping the intertidal topography from a single SWOT cycle at low tide. This allowed for the examination of the capability of SWOT to deliver accurate DEMs from a single pass at low tide conditions (Fig. 4.c and d for cycle 524 and 576 respectively). The importance of single-pass DEMs resides in the

SWOT low tide cycles and IGN LiDAR HD DEM difference (SWOT - IGN)

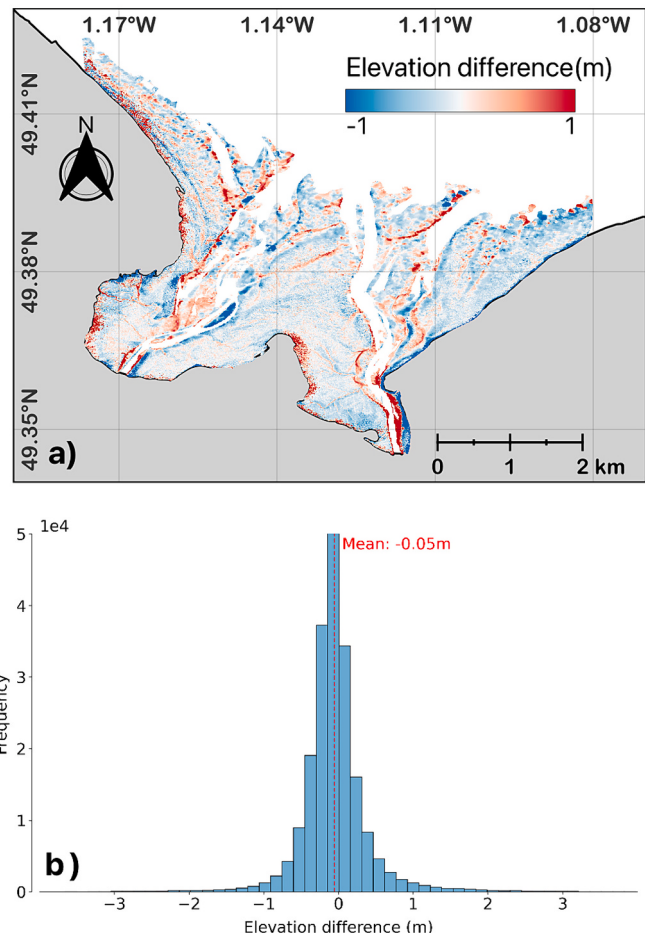


Fig. 6. (a) Elevation difference between IGN LiDAR HD DEM and SWOT low tide cycles DEM and (b) the corresponding histogram.

elimination of uncertainties related to topographical changes that might occur between the different passes used to build an aggregated DEM.

To assess the accuracy of SWOT-derived intertidal DEMs, airborne LiDAR data (LiDAR HD) alongside the two UAV LiDAR acquisitions of

April and August 2023 were used as benchmark datasets. SWOT DEMs were compared also to the waterline-derived DEM. Fig. 5 shows the comparison results between the three validation datasets and the SWOT DEM generated from data aggregation of low tide cycles. The latter demonstrated relatively low RMSEs and MAEs against LiDAR HD (0.49 m and 0.29 m) that reached an RMSE of 0.17 m and MAE of 0.13 m when compared to UAV LiDAR DEMs. It should be noted that by comparing SWOT's DEM against LiDAR HD for the area covered by the drone only, lower RMSE and MAE were obtained as well with values of 0.19 m and 0.15 m, respectively. This higher correspondence reached at a smaller scale may indicate that the middle part of the bay where the UAV acquisitions are made has a configuration that provides optimal conditions for satellite measurements. These conditions can be described as high flats where water drains more effectively (but the sand is still wet thus the high backscattered signal) with a minimal presence of ponds. Fig. 6 shows the spatial distribution of elevation difference between the LiDAR HD DEM and SWOT low tide cycles DEM. It confirms that the middle part of the bay is less prone to error, while higher differences are found close to water in channels. This could result from the misclassification of SWOT "open water" classified pixels by the k-means clustering algorithm and the inclusion of their elevations in bed elevation estimates, or from classifying SWOT "open water" pixels as mudflats where in reality there is a mix between water and sediment in SWOT's pixel. The R^2 values prove the high degree of correlation between SWOT and the LiDAR DEMs with a minimum value of 0.75 peaking at 0.94 (for the low tide cycles DEM). This correlation demonstrates that the 10-m DEMs based on SWOT HR data are reliable for mapping morphological features in intertidal areas that exceed this scale. The comparison with the waterline-derived DEM also shows good but lower correspondence, which is expected due to the inherent errors of the waterline method itself.

The SWOT DEM derived from all cycles demonstrated a slightly higher RMSEs and MAEs (Table A1 in Appendix), which could be the consequence of misclassification of mudflat pixels but also an indication of the influence of temporal variations in morphology on the aggregated DEMs accuracy. Furthermore, the results show a strong agreement between SWOT DEMs generated from single passes and the three LiDAR benchmarks, achieving RMSEs between 0.48 m and 0.71 m and MAEs between 0.29 m and 0.47 m against the LiDAR HD that covers the whole bay (lower errors when compared to UAV DEMs; Table A1). The differences in accuracy across single-pass DEMs indicate that certain conditions may impact the quality of the DEM. This could be the consequence of SWOT's sensitivity to specific environmental conditions (i.e. soil water content or rain). Nevertheless, SWOT single-pass DEMs

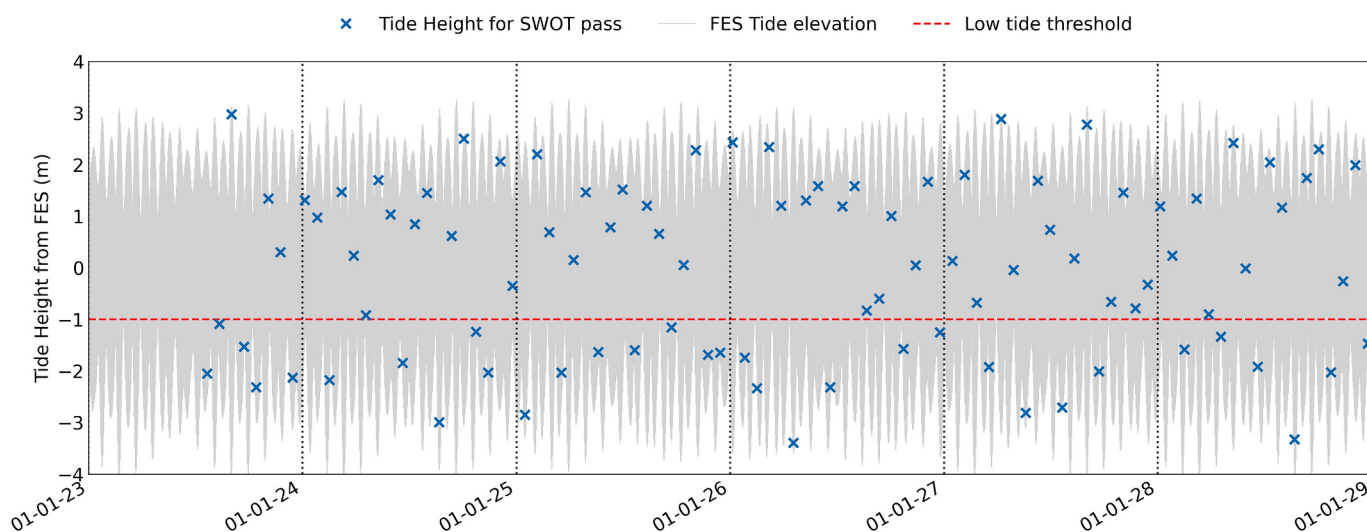


Fig. 7. SWOT scientific orbit passes according to tides predicted from FES2014 for the next 5 years over the Bay of Veys.

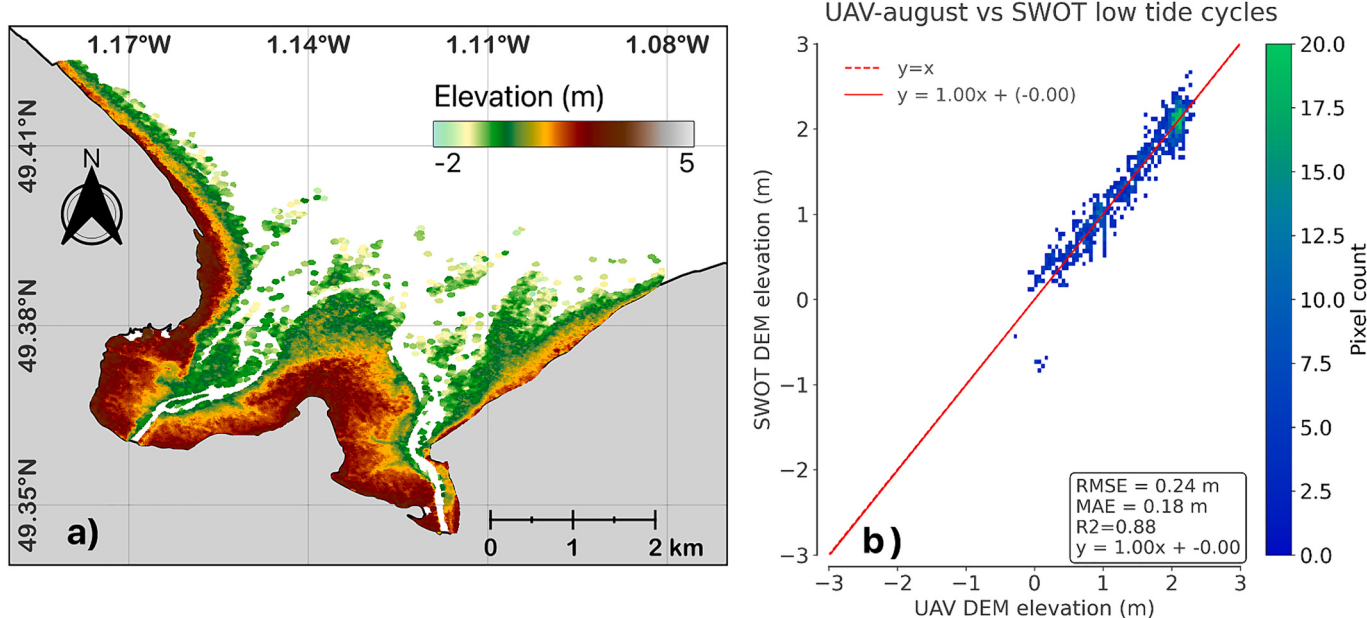


Fig. 8. (a) SWOT-derived intertidal DEM from available cycles at low tide (8, 11, and 17) of pass 42 of the scientific (nominal) orbit and (b) the comparison with UAV-August DEM.

show good accuracy and consistency.

During the nominal orbit phase, the occurrences of SWOT passes at low tides are less frequent due to the 21-day repeat cycle. Fig. 7 shows the expected SWOT passes over the Bay of Veys according to tidal height predicted from FES2014 (Carrère et al., 2016) for the next 5 years. For this specific study site, 4 to 7 low tide acquisitions are expected from SWOT. These acquisitions span different seasons, allowing the assessment of seasonal changes, particularly following highly energetic events that induce significant changes in the system.

Three cycles (8, 11, and 17) acquired at low tide for pass 42 of SWOT's scientific orbit covering the entire bay were available. They were used to generate an intertidal DEM in order to assess a non CALVAL performance. Fig. 8 shows the intertidal DEM after aggregating mudflat pixels from these 3 low tide cycles. The comparison with the UAV-August DEM shows an RMSE of 0.24 m and an MAE of 0.18 m. While the performance is good, the errors are higher compared to the CAVAL DEM. This can be explained by the longer time gap (4, 6, and 10 months) between the UAV acquisition in August and cycles 8, 11, and 17, or the higher number of low tide passes during CALVAL, which reduces noise and provides a more precise aggregated DEM. The performance of single-pass DEMs should be similar between CALVAL and the nominal phase, as single low tide passes are used to generate a single DEM.

6. Conclusions

SWOT was designed to provide a continuous spatio-temporal monitoring of sea surface height and inland water surface elevation. The study presented here is the first to demonstrate the capacity of SWOT to accurately measure the topography of intertidal areas based on interferometry, that is an unexpected opportunity provided by the mission, but an essential one for coastal areas. The validation was performed over the Bay of Veys intertidal area located within SWOT's CALVAL orbit. SWOT Intertidal DEMs derived from the L2_HR_PIXC product resulted in detailed representation of the topographic features of the bay with RMSEs and MAEs reaching 0.17 m and 0.13 m, respectively, after validation against benchmark datasets. As SWOT data and algorithms undergo further refinement, there is potential for more accurate intertidal topography products. The study also demonstrated that accurate DEMs can be generated from a single SWOT pass, opening new possibilities for

the future use of SWOT in studying the temporal variability of intertidal mudflats.

Since SWOT is based on near-nadir radar interferometry, a fundamental limitation is layover, i.e., the fact that nearby surfaces at the same distance from the radar may get mixed, as soon as the topographic slope in the ground range direction exceeds the incidence angle (varying from 1° in near-range to 4° in far range for SWOT). The Bay of Veys has a lower slope than 1°, thus layover was not a problem. In general, intertidal flats are gently sloped, but care must be taken when dealing with steep slopes or with intertidal areas close to steep landforms such as cliffs. Going forward, further testing of SWOT's ability to reconstruct the intertidal topography across different coastal systems, but also inland environments such as river floodplains and lake shores, is crucial to assess the sensitivity of SWOT products to varying site-specific conditions.

CRediT authorship contribution statement

Edward Salameh: Writing – review & editing, Writing – original draft, Visualization, Validation, Software, Project administration, Methodology, Investigation, Funding acquisition, Formal analysis, Data curation, Conceptualization. **Damien Desroches:** Writing – review & editing, Validation, Software, Methodology, Formal analysis, Data curation, Conceptualization. **Julien Deloffre:** Writing – review & editing, Validation, Software, Resources, Project administration, Investigation, Funding acquisition, Conceptualization. **Roger Fjørtoft:** Writing – review & editing, Supervision, Methodology, Investigation, Conceptualization. **Ernesto Tonatiuh Mendoza:** Writing – review & editing, Validation, Software, Investigation, Formal analysis, Data curation. **Imen Turki:** Writing – review & editing, Project administration, Investigation, Funding acquisition. **Laurent Froideval:** Writing – review & editing, Validation, Resources, Project administration, Investigation, Funding acquisition. **Romain Levaillant:** Validation, Software, Resources, Investigation, Data curation. **Simon Déchamps:** Writing – review & editing, Validation, Software, Methodology, Investigation, Formal analysis, Data curation. **Nicolas Picot:** Writing – review & editing, Supervision, Resources, Project administration, Methodology, Investigation, Funding acquisition. **Benoit Laignel:** Writing – review & editing, Supervision, Project administration, Investigation, Funding

acquisition. **Frédéric Frappart:** Writing – review & editing, Validation, Supervision, Methodology, Investigation, Formal analysis, Conceptualization.

Declaration of competing interest

The authors declare that they have no known competing financial interests or personal relationships that could have appeared to influence the work reported in this paper.

Data availability

All the datasets that support the findings of this study are available. SWOT level-2 high rate mode pixel cloud (L2_HR_PIXC) product is available on <https://hydroweb.next.theia-land.fr/> and <https://search.earthdata.nasa.gov/>. The version used in this study is PIA1 CRID version manually corrected from crossover errors, and we recommend

that the user use the latest PGC0 CRID version. The IGN LiDAR HD dataset is publicly available on <https://diffusion-lidarhd.ign.fr/>. The UAV-derived DEM are available for 1 m and 10 m resolution via doi:[10.82233/IPSIXN](https://doi.org/10.82233/IPSIXN), and the raw UAV LiDAR acquisitions are available upon request.

Acknowledgements

This work was supported by the French Space Agency CNES (Centre National d'Etudes Spatiales) in the framework of the TOSCA program SWOT3MC/CALVAL. We thank the anonymous reviewers for their valuable feedback and suggestions, which have significantly improved this manuscript. We extend our gratitude to the Direction Départementale des Territoires et de la Mer (DDTM de la manche) for granting us the authorization to conduct measurements in the Bay of Veys, Normandy.

Appendix A. Appendix

Table A1

Comparative analysis between SWOT DEMs and IGN LiDAR HD, UAV April, UAV August, and the Waterline method.

SWOT DEMs	RMSE*	MAE*	R2*	Slope*	Intercept*
SWOT all cycles	0.74/0.23/0.20/0.83	0.41/0.18/0.14/0.54	0.74/0.90/0.93/0.53	0.93/0.98/1.01/1.08	0.17/-0.08/-0.01/0.31
SWOT low tide cycles	0.49/0.23/0.17/0.60	0.29/0.18/0.13/0.43	0.89/0.90/0.94/0.75	0.97/0.99/1.02/1.11	-0.05/-0.12/-0.05/0.09
SWOT cycle 488	0.58/0.29/0.21/0.60	0.38/0.26/0.18/0.36	0.52/0.78/0.88/0.29	0.69/0.96/0.97/0.78	0.27/-0.18/-0.09/0.43
SWOT cycle 489	0.51/0.30/0.23/0.50	0.32/0.25/0.18/0.35	0.80/0.82/0.90/0.76	0.88/0.96/0.99/0.98	-0.03/-0.17/-0.10/0.16
SWOT cycle 490	0.53/0.26/0.28/0.63	0.31/0.19/0.21/0.49	0.73/0.86/0.83/0.49	0.82/1.01/1.04/0.94	0.30/0.03/0.09/0.47
SWOT cycle 500	0.53/0.34/0.26/0.45	0.35/0.29/0.22/0.33	0.70/0.78/0.87/0.73	0.79/0.98/1.01/0.91	0.11/-0.21/-0.15/0.27
SWOT cycle 501	0.48/0.28/0.24/0.52	0.29/0.21/0.17/0.38	0.82/0.85/0.89/0.73	0.87/1.09/1.11/0.98	0.08/-0.27/-0.20/0.26
SWOT cycle 502	0.53/0.28/0.22/0.57	0.31/0.22/0.17/0.40	0.81/0.85/0.90/0.71	0.90/0.94/0.97/1.01	0.04/-0.09/-0.02/0.22
SWOT cycle 503	0.63/0.28/0.27/0.70	0.36/0.21/0.19/0.47	0.66/0.85/0.86/0.44	0.86/1.06/1.09/0.99	0.17/-0.14/-0.07/0.34
SWOT cycle 511	0.55/0.39/0.32/0.47	0.38/0.30/0.23/0.34	0.72/0.67/0.78/0.75	0.82/1.14/1.14/0.91	-0.00/-0.46/-0.34/0.2
SWOT cycle 515	0.53/0.32/0.23/0.50	0.34/0.26/0.18/0.34	0.79/0.81/0.90/0.76	0.85/0.92/0.95/0.97	-0.01/-0.13/-0.06/0.16
SWOT cycle 516	0.53/0.29/0.21/0.56	0.32/0.25/0.17/0.38	0.75/0.83/0.91/0.64	0.84/0.96/0.98/0.94	0.09/-0.18/-0.10/0.28
SWOT cycle 523	0.60/0.34/0.27/0.60	0.37/0.27/0.21/0.41	0.69/0.76/0.85/0.60	0.80/0.98/0.99/0.92	0.17/-0.22/-0.13/0.32
SWOT cycle 524	0.49/0.39/0.36/0.60	0.32/0.31/0.26/0.42	0.88/0.73/0.78/0.75	1.01/1.07/1.08/1.14	-0.22/-0.30/-0.20/-0.07
SWOT cycle 525	0.49/0.33/0.26/0.48	0.31/0.26/0.19/0.37	0.77/0.79/0.87/0.73	0.83/1.03/1.06/0.93	0.11/-0.28/-0.21/0.31
SWOT cycle 536	0.71/0.17/0.15/0.74	0.40/0.14/0.11/0.46	0.55/0.92/0.94/0.30	0.71/0.93/0.94/0.84	0.38/0.04/0.12/0.47
SWOT cycle 538	0.56/0.24/0.20/0.63	0.31/0.17/0.12/0.45	0.73/0.89/0.92/0.56	0.88/1.05/1.08/0.98	0.12/-0.21/-0.14/0.31
SWOT cycle 539	0.51/0.19/0.14/0.58	0.29/0.15/0.11/0.43	0.73/0.93/0.96/0.54	0.84/0.96/0.98/0.94	0.20/-0.06/0.01/0.37
SWOT cycle 540	0.55/0.25/0.19/0.58	0.32/0.21/0.15/0.42	0.71/0.87/0.92/0.59	0.82/1.01/1.04/0.91	0.16/-0.20/-0.14/0.35
SWOT cycle 549	0.67/0.41/0.34/0.66	0.41/0.33/0.26/0.43	0.71/0.67/0.78/0.63	0.92/1.03/1.06/1.05	-0.06/-0.36/-0.29/0.11
SWOT cycle 550	0.65/0.29/0.31/0.79	0.41/0.22/0.24/0.61	0.72/0.84/0.82/0.46	0.91/0.97/0.99/1.03	0.34/0.09/0.15/0.52
SWOT cycle 551	0.69/0.29/0.24/0.76	0.37/0.23/0.18/0.48	0.63/0.84/0.89/0.44	0.87/0.96/0.99/0.96	0.10/-0.12/-0.05/0.31
SWOT cycle 562	0.64/0.32/0.28/0.72	0.37/0.24/0.20/0.49	0.68/0.81/0.85/0.45	0.85/0.93/0.96/0.98	0.18/-0.02/0.04/0.35
SWOT cycle 563	0.56/0.17/0.16/0.64	0.31/0.13/0.13/0.48	0.76/0.94/0.95/0.57	0.87/0.96/0.98/0.98	0.18/0.01/0.07/0.37
SWOT cycle 564	0.54/0.23/0.23/0.64	0.31/0.17/0.18/0.50	0.77/0.90/0.90/0.60	0.87/0.99/1.01/0.98	0.23/-0.04/0.03/0.43
SWOT cycle 565	0.63/0.26/0.25/0.72	0.36/0.20/0.20/0.53	0.66/0.87/0.88/0.39	0.85/0.92/0.94/0.98	0.30/0.07/0.13/0.45
SWOT cycle 574	0.56/0.41/0.42/0.63	0.33/0.30/0.28/0.45	0.70/0.55/0.55/0.52	0.82/1.35/1.35/0.92	0.21/-0.59/-0.45/0.39
SWOT cycle 575	0.67/0.29/0.29/0.77	0.38/0.21/0.22/0.55	0.66/0.82/0.82/0.41	0.79/1.03/1.03/0.90	0.38/-0.09/0.02/0.54
SWOT cycle 576	0.52/0.22/0.19/0.62	0.30/0.18/0.15/0.42	0.87/0.90/0.93/0.74	0.98/1.00/1.02/1.12	0.01/-0.12/-0.05/0.18
SWOT cycle 577	0.84/0.23/0.21/0.94	0.47/0.18/0.16/0.60	0.62/0.90/0.91/0.30	0.95/0.94/0.96/1.12	0.08/0.00/0.07/0.21

* LiDAR HD / UAV April / UAV August / Waterline.

References

- Arthur, D., Vassilvitskii, S., 2007. K-Means++: The Advantages of Careful Seeding, in: Proceedings of the Eighteenth Annual ACM-SIAM Symposium on Discrete Algorithms. Society for Industrial and Applied Mathematics.
- Aviso, 2023. SWOT orbit [WWW Document]. <https://www.aviso.altimetry.fr/en/missions/current-missions/swot/orbit.html>.
- Benveniste, J., Cazenave, A., Vignudelli, S., Fenoglio-Marc, L., Shah, R., Almar, R., Andersen, O., Birol, F., Bonnefond, P., Bouffard, J., Calafat, F., Cardellach, E., Cipollini, P., Le Cozannet, G., Dufau, C., Fernandes, M.J., Frappart, F., Garrison, J., Gommenginger, C., Han, G., Hoyer, J.L., Kourafalou, V., Leuliette, E., Li, Z., Loisel, H., Madsen, K.S., Marcos, M., Mellet, A., Meyssignac, B., Pascual, A., Passaro, M., Ribó, S., Scharroo, R., Song, Y.T., Speich, S., Wilkin, J., Woodworth, P., Wöppelmann, G., 2019. Requirements for a coastal hazards observing system. *Front. Mar. Sci.* 6, 348. <https://doi.org/10.3389/fmars.2019.00348>.
- Biancamaria, S., Lettenmaier, D.P., Pavelsky, T.M., 2016. The SWOT Mission and its Capabilities for Land Hydrology. Springer, Cham, pp. 117–147. https://doi.org/10.1007/978-3-319-32449-4_6.
- Carrère, L., Lyard, F., Cancet, M., Guillot, A., Picot, N., 2016. FES 2014, a new tidal model—Validation results and perspectives for improvements. In: *ESA Living Planet Symposium*, pp. 9–13.
- Deroïn, J.-P., 2012. Combining ALOS and ERS-2 SAR data for the characterization of tidal flats. Case study from the Baie des Veys, Normandy, France. *Int. J. Appl. Earth Obs. Geoinf.* 18, 183–194. <https://doi.org/10.1016/J.JAG.2012.01.019>.
- Fjørtoft, R., Gaudin, J.-M., Pourthié, N., Lalaurie, J.-C., Mallet, A., Nouvel, J.-F., Martinot-Lagarde, J., Oriot, H., Borderies, P., Ruiz, C., Daniel, S., 2014. KaRin on SWOT: characteristics of near-nadir Ka-band interferometric SAR imagery. *IEEE*

- Trans. Geosci. Remote Sens. 52, 2172–2185. <https://doi.org/10.1109/TGRS.2013.2258402>.
- Fu, L.L., Pavelsky, T., Cretaux, J.F., Morrow, R., Farrar, J.T., Vaze, P., Sengenes, P., Vinogradova-Shiffer, N., Sylvestre-Baron, A., Picot, N., Dibarboure, G., 2024. The surface water and ocean topography Mission: a breakthrough in radar remote sensing of the ocean and land surface water. Geophys. Res. Lett. 51 <https://doi.org/10.1029/2023GL107652>.
- Gens, R., Van Genderen, J.L., 1996. Review article SAR interferometry—issues, techniques, applications. Int. J. Remote Sens. 17, 1803–1835. <https://doi.org/10.1080/01431169608948741>.
- Grangeré, K., Ménèsguen, A., Lefebvre, S., Bacher, C., Pouvreau, S., 2009. Modelling the influence of environmental factors on the physiological status of the Pacific oyster *Crassostrea gigas* in an estuarine embayment; the Baie des Veys (France). J. Sea Res. 62, 147–158. <https://doi.org/10.1016/J.SEARES.2009.02.002>.
- IGN, 2022. LIDAR HD [WWW Document]. <https://geoservices.ign.fr/lidarhd#telechargementclassifiees>.
- IGN, 2023. FAQ LIDAR HD [WWW Document]. <https://geoservices.ign.fr/documentation/donnees/alti/lidarhd/faq-lidarhd>.
- IGN, 2023a. LiDAR HD Version 1.0 - Descriptif de contenu des nuages de points LiDAR. IGN, 2024. Avancement Acquisitions LiDAR HD au 22 Janvier 2024 [WWW Document]. https://macarte.ign.fr/carte/322ea69dab4c7e5afabc6ec7043b5994/acquisition_nslidarhd.
- JPL D-105504, 2023. SWOT Algorithm Theoretical Basis Document: L2 HR PIXC Jet Propulsion Laboratory Internal Document.
- JPL D-56411, 2023. Level 2 KaRIn high rate water mask pixel cloud product.
- Lafforgue, M., Gerard, L., Vieillard, C., Breton, M., 2018. Modelling of enterobacterial loads to the Baie des Veys (Normandy, France). Int. J. Hyg. Environ. Health 221, 847–860. <https://doi.org/10.1016/J.IJHEH.2018.04.008>.
- Laiguel, B., Vignudelli, S., Almar, R., Becker, M., Bentamy, A., Benveniste, J., Birol, F., Frappart, F., Idier, D., Salameh, E., Passaro, M., Menende, M., Simard, M., Turki, E.I., Verpoorter, C., 2023. Observation of the coastal areas, Estuaries and Deltas from space. Surv. Geophys. <https://doi.org/10.1007/s10712-022-09757-6>.
- Lee, S.-K., Ryu, J.-H., 2017. High-accuracy tidal flat digital elevation model construction using TanDEM-X science phase data. IEEE J. Sel. Top. Appl. Earth Obs. Remote Sens. 10, 2713–2724. <https://doi.org/10.1109/JSTARS.2017.2656629>.
- Lobry, S., Denis, L., Williams, B., Fjortoft, R., Tupin, F., 2019. Water detection in SWOT HR images based on multiple Markov random fields. IEEE J. Sel. Top. Appl. Earth Obs. Remote Sens. 12, 4315–4326. <https://doi.org/10.1109/JSTARS.2019.294788>.
- Mason, D.C., Davenport, L.J., Robinson, G.J., Flather, R.A., McCartney, B.S., 1995. Construction of an inter-tidal digital elevation model by the “water-line” method. Geophys. Res. Lett. 22, 3187–3190.
- Masselink, G., Gehrels, R., 2015. Coastal environments and global change. In: Masselink, G., Gehrels, R. (Eds.), Coastal Environments and Global Change. John Wiley & Sons, Ltd, Chichester, UK, pp. 1–27. <https://doi.org/10.1002/9781119117261.ch1>.
- Murray, N.J., Phinn, S.R., DeWitt, M., Ferrari, R., Johnston, R., Lyons, M.B., Clinton, N., Thau, D., Fuller, R.A., 2019. The global distribution and trajectory of tidal flats. Nature 565, 222–225. <https://doi.org/10.1038/s41586-018-0805-8>.
- Salameh, E., Frappart, F., Almar, R., Baptista, P., Heygster, G., Lubac, B., Raucoules, D., Almeida, L.P., Bergsma, E.W.J., Capo, S., De Michele, M.D., Idier, D., Li, Z., Marieu, V., Poupardin, A., Silva, P.A., Turki, I., Laiguel, B., 2019. Monitoring beach topography and nearshore bathymetry using Spaceborne remote sensing: a review. Remote Sens. 11 <https://doi.org/10.3390/rs11192212>.
- Salameh, E., Frappart, F., Turki, I., Laiguel, B., 2020. Intertidal topography mapping using the waterline method from Sentinel-1 & -2 images: the examples of Arcachon and Veys bays in France. ISPRS J. Photogramm. Remote Sens. 163 <https://doi.org/10.1016/j.isprsjprs.2020.03.003>.
- Salameh, E., Frappart, F., Desroches, D., Turki, I., Carbone, D., Laiguel, B., 2021. Monitoring intertidal topography using the future SWOT (surface water and ocean topography) mission. Remote Sens. Appl. 23 <https://doi.org/10.1016/j.rsase.2021.100578>.
- Shepard, D., 1968. A Two-Dimensional Interpolation Function for Irregularly-Spaced Data, in Proceedings of the 1968 23rd ACM National Conference. ACM, New York, USA, pp. 517–524. <https://doi.org/10.1145/800186.810616>.
- SHOM, 2014. Modèle numérique d'évolution de l'océan HYCOM [WWW Document]. http://services.data.shom.fr/geonetwork/srv/api/records/OCEANO_MODELE_HYCOM.xml.
- Timsit, O., Sylvand, B., Lefevre, J.-C., 2004. Évolution du macrozoobenthos intertidal de la baie des Veys de 1985 à 2000. C. R. Biol. 327, 51–64. <https://doi.org/10.1016/J.CRVI.2003.11.002>.